Effects of electric field on vibrational resonances in Hindmarsh–Rose neuronal systems for signal detection

Xiaoxia Li(李晓霞)[1,3,†], Xiaopeng Xue(薛小鹏)[2], Dongjie Liu(刘栋杰)[1,3], Tianyi Yu(余天意)[1,3], Qianqian He(何倩倩)[2], and Guizhi Xu(徐桂芝)[1,2,3]

[1] *State Key Laboratory of Reliability and Intelligence of Electrical Equipment, Hebei University of Technology, Tianjin* 300130, *China*
[2] *School of Health Sciences & Biomedical Engineering, Hebei University of Technology, Tianjin* 300130, *China*
[3] *Key Laboratory of Electromagnetic Field and Electrical Apparatus Reliability of Hebei Province, Hebei University of Technology, Tianjin* 300130, *China*

(Received 16 August 2022; revised manuscript received 29 September 2022; accepted manuscript online 21 October 2022)

Changes in the concentration of charged ions in neurons can generate induced electric fields, which can further modulate cell membrane potential. In this paper, Fourier coefficients are used to investigate the effect of electric field on vibrational resonance for signal detection in a single neuron model and a bidirectionally coupled neuron model, respectively. The study found that the internal electric field weakens vibrational resonance by changing two factors, membrane potential and phase-locked mode, while the periodic external electric field of an appropriate frequency significantly enhances the vibrational resonance, suggesting that the external electric field may play a constructive role in the detection of weak signals in the brain and neuronal systems. Furthermore, when the coupling of two neurons is considered, the effect of the electric field on the vibrational resonance is similar to that of a single neuron. The paper also illustrates the effect of electric field coupling on vibrational resonance. This study may provide a new theoretical basis for understanding information encoding and transmission in neurons.

Keywords: electric field, Fourier-coefficient, neuronal dynamics, vibrational resonance

PACS: 87.19.ll, 87.18.Sn, 87.19.ln, 87.19.lg **DOI:** 10.1088/1674-1056/ac9cc0

1. Introduction

Stochastic resonance (SR) was first proposed by Benzi *et al.*[1,2] in the study of climate change, and it was subsequently used to describe the enhancement of the system output by internal or external noise in nonlinear systems.[3] SR is widely used in physics,[4,5] interdisciplinary,[6–8] and engineering applications.[9,10] With the deepening of research, scholars have discovered a new form of resonance, vibratory resonance (VR).[11] When the nonlinear system is affected by the dual-frequency signal, the high-frequency periodic signal will replace the noise to amplify the weak signal. Zaikin *et al.* studied the vibrational resonance of a space-expanded system of coupled noise oscillators under dual-frequency periodic force, and the noise-induced phase transition and vibrational resonance together optimize the signal processing.[12] Chizhevsky *et al.* studied VR in bistable vertical cavity lasers, where the detection of low-level signals depends on the magnitude of the applied high-frequency modulation.[13] Ghosh *et al.* studied the nonlinear response of bistable systems driven by high-frequency forces to low-frequency weak fields, and showed that rapidly changing time oscillations break the spatial symmetry of the centrosymmetric potential.[14] In addition, the internal or external chaotic signals of nonlinear systems can also enhance the system's response to weak signals.[15] The amplification effect of this chaotic signal on the weak signal is called chaotic resonance (CR). Nobukawa *et al.* proposed that the method of reducing orbital area is applied to the nervous system composed of excitatory and inhibitory neurons and induced chaotic resonance, in which external noise exhibits the effect of reducing and enhancing the signal response.[16] Baysal *et al.* studied the effect of chaotic activity on the collective behavior of Hodgkin–Huxley (HH) neurons in small-world networks and observed chaotic resonances in both individual neurons and neuron networks.[17] Yao *et al.* observed utilizing the interaction of chaotic signals and periodic forces and the coupling-generated CR in a coupled bistable system that can operate robustly as a specific logic gate in an optimal window of chaotic signal strengths.[18]

Neurons transmit and encode information in the form of firing.[19–21] The HH classical neuron model has reliable mathematical models and physical explanations, and provides a feasible method for studying different neuronal electrical activities and brain operating mechanisms. As the main feature of electrical activity, the membrane potential of neurons can exhibit resting, spiking, bursting, and chaotic states and nonlinear circuits can be constructed for research.[22,23] In addition, scholars have successively proposed some simplified neuron models, such as the two-parameter FitzHugh–Nagumo (FHN) neuron model,[24] the Morris–Lecar (ML) neuron model inspired by barnacle muscle fibers,[25] the Hindmarsh–Rose (HR) neuron model obtained from snail neurons,[26] and the

[†]Corresponding author. E-mail: lixiaoxia@hebut.edu.cn

© 2023 Chinese Physical Society and IOP Publishing Ltd

Prescott neuron model with slow recovery variables by improving the ML neuron model.[27] The simplified model facilitates bifurcation studies and the construction of nonlinear neural circuits and preserves complex neuronal electrical activity patterns. As a way of information processing, the resonance phenomenon is ubiquitous in biological neuronal systems.[28,29] In recent years, the effects of parameters of neuronal systems and external stimuli on the resonance of individual neurons and different coupled neural networks have been extensively studied. Song *et al.* studied CR in HH neuron models with self-synapses, which exhibited different firing behaviors under subthreshold and suprathreshold inputs.[30] Han *et al.* studied VR in parallel arrays, where local connections play a key role in weak signal detection.[31] Li *et al.* discussed stochastic multi-resonance in small-world FHN neuronal networks, showing that the occurrence of stochastic multi-resonance is closely related to the period of the subthreshold signal and the noise-induced average period of the neuronal network.[32]

For biological neurons, the electric charges flowing between the membranes will cause fluctuations in the concentration distribution of charged ions, and the time-varying electromagnetic fields generated by such fluctuations will affect the electrical activity of neurons.[33] Lv *et al.* established a four-variable HR neuron model, and the electromagnetic induction generated by the change of ion concentration was realized by a magnetron memristor.[34] In addition, the effects of external electromagnetic fields on biological nerve tissue have also been widely studied.[35–37] Based on the study of neuronal dynamics by electromagnetic fields, the treatment of neurodegenerative diseases by external magnetic stimulation has been applied in clinical medicine, such as Alzheimer's disease[38,39] and epilepsy.[40,41] Therefore, it is of great practical significance to explore the effect of electromagnetic fields and different factors on the electrical activity of neurons. In recent years, many works have investigated the resonance of neurons modulated by various factors in the electromagnetic environment through experimental and numerical methods. Yao *et al.* by studying the resonance characteristics of HH neurons under magnetic flux noise concluded that an appropriate external electromagnetic field can partially restore the damaged information encoding ability, while too strong electromagnetic radiation can lead to neurological disorders.[42] Ge *et al.* studied VR in FHN neuronal networks under electromagnetic induction, and high-frequency stimulation played an important role in the collective activity of the network.[43] Baysal *et al.* found that electromagnetic induction can reduce the energy required for VR to occur in neuronal networks, but reduce the resonance peak, which means that a magnetic flux of appropriate strength can enhance the detection of weak signals by the system.[44] In addition, the transmembrane flow of charged ions can also generate polarization phenomena on the cell membrane,[45,46] thereby creating an induced electric field in the medium. Deep brain stimulation (DBS)[47] is an effective method for the treatment of neurological diseases. Its principle is to suppress the abnormal electrical activity of neurons by implanting electrodes in specific nerve groups and giving low-frequency or high-frequency electrical stimulation. Today, electrical stimulation can treat a variety of diseases such as epilepsy, Parkinson and obsessive–compulsive disorder, and has good results in improving the quality of life of patients. However, the effect of electrical stimulation on the electrical activity of neurons and the specific therapeutic mechanism still needs further exploration.[48,49] The HR neuron model, as a derived model of the HH neuron, is widely used in the field of neuroscience research. Consider the mathematical model of a single HR neuron as a nonlinear system with more parameters than other simplified neuron models, capable of simulating major neural behaviors such as spiking, bursting, and chaos.[34] Therefore, this paper is inspired by the work done by Wouapi *et al.* to consider the effects of internal and external electric fields on VR in a fourth-order HR neuron model with field variables.[50]

The structure of the paper is as follows. In Section 2, a single HR neuron model with electric field is introduced, and HR neurons model coupled with electric field is also included. Section 3 presents the main numerical results. Finally, Section 4 gives our conclusions.

2. Model and methods

2.1. Hindmarsh–Rose model

The general HR neuron model is described by a set of three-dimensional nonlinear differential equations, written as:[25]

$$\begin{aligned}\frac{\mathrm{d}x}{\mathrm{d}t} &= y - ax^3 + bx^2 - z + I_{\mathrm{ext}},\\ \frac{\mathrm{d}y}{\mathrm{d}t} &= c - dx^2 - y,\\ \frac{\mathrm{d}z}{\mathrm{d}t} &= r\left[s\left(x - \chi_{\mathrm{e}}\right) - z\right],\end{aligned} \tag{1}$$

where x represents the cell membrane potential, y is the recovery variable associated with the rapid rate of change of sodium and potassium ion currents, and z stands for the adaptation variable associated with the slow change of the ion channel. $I_{\mathrm{ext}} = A\cos(\omega t) + B\cos(N_1\omega t)$ is the external stimulation current, $A\cos(\omega t)$ is the low frequency signal (LFS), $B\cos(N_1\omega t)$ is the high frequency signal (HFS), and N_1 is the frequency ratio of HFS to LFS. The other parameters a, b, c, d, r, and s are the internal characteristic parameters of the system, and χ_{e} is the stable points of the system.

2.2. Coupled Hindmarsh–Rose model without electric field

Hindmarsh–Rose model of electrical synaptic coupling reads

$$\begin{aligned}
\frac{\mathrm{d}x_1}{\mathrm{d}t} &= y_1 - ax_1^3 + bx_1^2 - z_1 + g_1(x_2 - x_1) \\
&\quad + A\cos(\omega t) + B\cos(N_1\omega t), \\
\frac{\mathrm{d}y_1}{\mathrm{d}t} &= c - dx_1^2 - y_1, \\
\frac{\mathrm{d}z_1}{\mathrm{d}t} &= r\left[s\left(x - \chi_{\mathrm{e}}\right) - z\right], \\
\frac{\mathrm{d}x_2}{\mathrm{d}t} &= y_2 - ax_2^3 + bx_2^2 - z_2 + g_1(x_1 - x_2) + B\cos(N_1\omega t), \\
\frac{\mathrm{d}y_2}{\mathrm{d}t} &= c - dx_2^2 - y_2, \\
\frac{\mathrm{d}z_2}{\mathrm{d}t} &= r\left[s\left(x - \chi_{\mathrm{e}}\right) - z\right], \qquad (2)
\end{aligned}$$

where $g_1(x_2 - x_1)$ is the electrical synaptic coupling between two neurons and g_1 represents the coupling strength of the electrical synapse. We study the VR phenomenon in coupled neurons under local stimulation by allowing each neuron to be stimulated by the same high-frequency signal.[51]

2.3. Hindmarsh–Rose model with electric field

When charged ions inside and outside the cell membrane move across the membrane, an electric field (EF) is induced across the membrane. The fluctuation of the membrane potential is described by the electric field variable E. Assuming that the size of the neurons cell membrane is S, and the charge on the neurons cell membrane is Q, we can obtain the electric field and potential on the cell membrane as follows:

$$E = \frac{Q}{2\varepsilon S}, \quad \Delta V = RE = E\sqrt{S}, \qquad (3)$$

where ε represents the dielectric constant related to the internal properties of the cell. R represents the average radius of cells under a uniform EF, and E is the strength of the uniform electric field. ΔV represents the potential difference across the cell membrane.

To reveal the effects of electric fields on neuronal dynamics, we introduced electric field variables into the HR neuron model. When we consider the influence of the EF, the improved Hindmarsh–Rose model can be written as[44]

$$\begin{aligned}
\frac{\mathrm{d}x}{\mathrm{d}t} &= y - ax^3 + bx^2 - z + A\cos(\omega t) + B\cos(N_1\omega t), \\
\frac{\mathrm{d}y}{\mathrm{d}t} &= c - dx^2 - y + RE, \\
\frac{\mathrm{d}z}{\mathrm{d}t} &= r\left[s\left(x - \chi_{\mathrm{e}}\right) - z\right], \\
\frac{\mathrm{d}E}{\mathrm{d}t} &= my + E_{\mathrm{ext}}, \qquad (4)
\end{aligned}$$

where $m = (1/2)\varepsilon S$ is used to describe the polarization characteristics. R is the size of the cell radius considering the spherical shape. Since fast currents are more sensitive to electric fields than slow currents, the term is added to the second term.[46] Field variable as a new variable to estimate the transmembrane motion of ions and changes in membrane potential. $E_{\mathrm{ext}} = C\cos(N_2\omega t)$ is the external electric field, which can be in the form of noise-like radiation or periodic modulation, C is the intensity of the external EF and N_2 is the ratio of the external EF to the frequency of the LFS.

2.4. Coupled Hindmarsh–Rose model with electric field

The coupled Hindmarsh–Rose model considering the influence of EF is described as

$$\begin{aligned}
\frac{\mathrm{d}x_1}{\mathrm{d}t} &= y_1 - ax_1^3 + bx_1^2 - z_1 + g_1(x_2 - x_1) \\
&\quad + A\cos(\omega t) + B\cos(N_1\omega t), \\
\frac{\mathrm{d}y_1}{\mathrm{d}t} &= c - dx_1^2 - y_1 + RE, \\
\frac{\mathrm{d}z_1}{\mathrm{d}t} &= r\left[s\left(x - \chi_{\mathrm{e}}\right) - z\right], \\
\frac{\mathrm{d}E_1}{\mathrm{d}t} &= my_1 + E_{\mathrm{ext}} + g_2(E_2 - E_1), \\
\frac{\mathrm{d}x_2}{\mathrm{d}t} &= y_2 - ax_2^3 + bx_2^2 - z_2 + g_1(x_1 - x_2) + B\cos(N_1\omega t), \\
\frac{\mathrm{d}y_2}{\mathrm{d}t} &= c - dx_2^2 - y_2 + RE, \\
\frac{\mathrm{d}z_2}{\mathrm{d}t} &= r\left[s\left(x - \chi_{\mathrm{e}}\right) - z\right], \\
\frac{\mathrm{d}E_2}{\mathrm{d}t} &= my_2 + E_{\mathrm{ext}} + g_2(E_1 - E_2), \qquad (5)
\end{aligned}$$

where $g_2(E_2 - E_1)$ represents the electric field coupling between two neurons, and g_2 is the strength of the electric field coupling. We exposed both neurons to the same high-frequency signal and an external electric field.

2.5. Fourier coefficient

Fourier coefficients can accurately measure the amount of information in the signal transmitted in the outer period.[52] As a measure of VR, we used Fourier coefficients Q to quantify neuronal responses to low-frequency signals. Q is defined as

$$\begin{aligned}
Q &= \sqrt{Q_{\sin}^2 + Q_{\cos}^2}, \\
Q_{\sin} &= \frac{2}{nT}\int_{T_0}^{T_0+nT} x(t)\sin(\omega t)\,\mathrm{d}t, \\
Q_{\cos} &= \frac{2}{nT}\int_{T_0}^{T_0+nT} x(t)\cos(\omega t)\,\mathrm{d}t, \qquad (6)
\end{aligned}$$

where $T = 2\pi/\omega$, n is the number of calculation cycles. In order to study the response of neurons to low-frequency signals in a macroscopic time range, this paper selects $n = 500$.

When the output is synchronized with a low-frequency signal, the signal transfer is enhanced, resulting in higher response amplitude Q.

The fourth-order Runge–Kutta method is used, the time step is set to 0.01, and the other parameters are set as $a = 1$, $b = 3$, $c = 1$, $d = 5$, $r = 0.006$, $s = 4$, $\chi_e = -1.56$, $A = 0.3$, $\omega = 0.0314$, $R = 0.00001$, and $m = 0.1$.

3. Result

3.1. VR in single Hindmarsh–Rose neuron model

First, we investigated the effect of internal EF on the responses of single neuron to the LFS. Figure 1 illustrates the value of Q *versus* B for a single HR neuron at different HFS frequencies. It can be seen that a variety of VR phenomena can be observed with or without the influence of EF. Multiple vibration resonances (MVR) can be observed at low N_1, and with the N_1 increasing, the number of resonance peaks decreases, and the neuronal response amplitude Q increases. This suggests that the frequency of the HFS is an important factor affecting the response of HR neurons to LFS. And when the ratio N_1 of HFS to LFS frequency is small, neurons can detect weak signals at multiple HFS intensities.

Furthermore, HR neurons exposed to EF had a smaller response Q (red line) than HR neurons unaffected by the EF (black line) for the same frequency ratio N_1, suggesting that the internal EF has an inhibitory effect on VR. We also found that when the effect of EF on HR neurons was considered, the HFS amplitude B required to achieve the maximum response Q was larger, implying that more energy was required for VR in neurons exposed to EF.

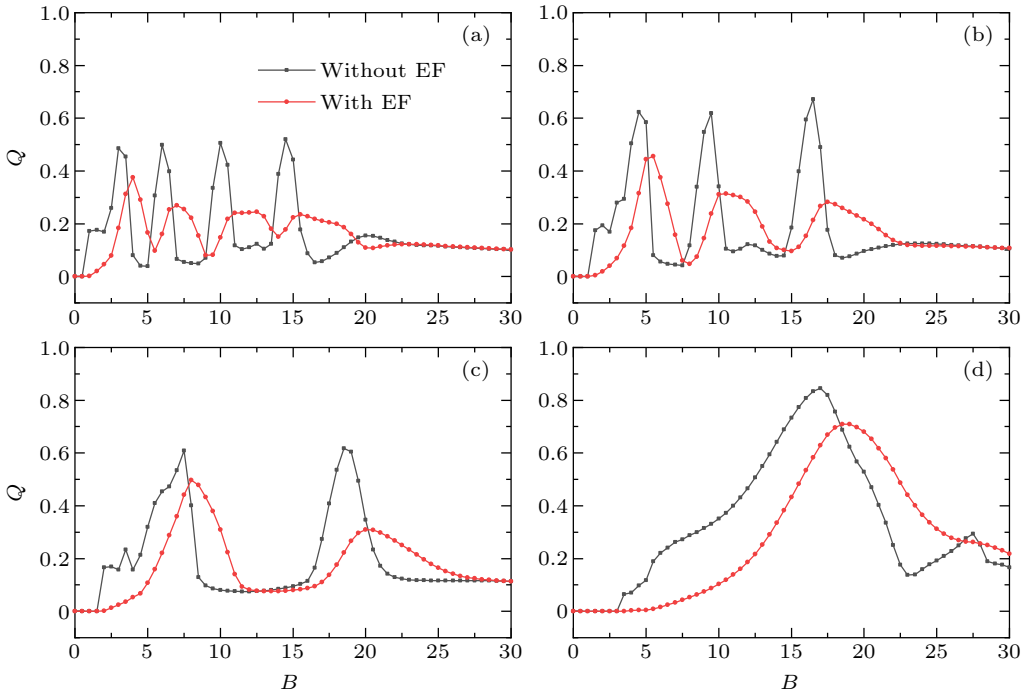


Fig. 1. Neuronal responses Q to the amplitude B of HFS at different frequency ratios N_1, without and with EF, $A = 0.3$, $\omega = 0.0314$, $R = 0.00001$, $m = 0.1$; (a) $N_1 = 9$, (b) $N_1 = 12$, (c) $N_1 = 18$, (d) $N_1 = 80$.

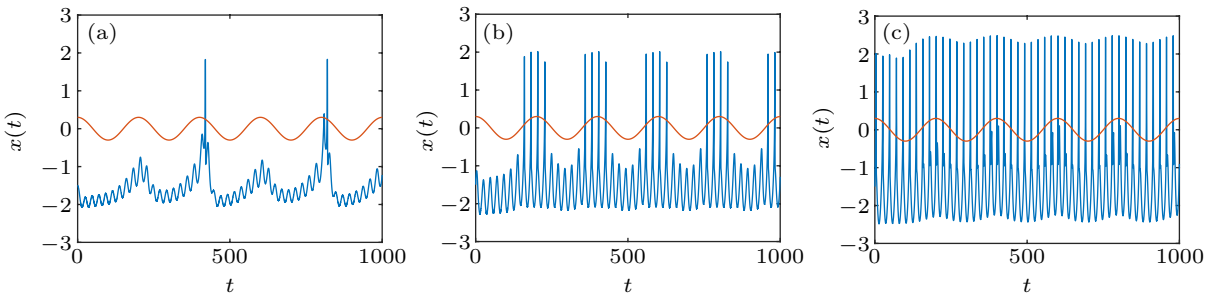


Fig. 2. Time evolution of membrane potential and LFS for different values of HFS amplitude B; (a) $B = 1$, (b) $B = 3$, (c) $B = 5$; without EF and $N_1 = 9$, $A = 0.3$, $\omega = 0.0314$, $R = 0.00001$, $m = 0.1$.

The evolutions of membrane potential and LFS with time are shown in Fig. 2. As shown in Fig. 2(a), for a relatively small HFS amplitude (for $B = 1$), the neuron has only individual action potentials, the response to the LFS is low, and only a small amount of information can be transmitted. As shown in Fig. 2(b), with the increase of the HFS amplitude (for $B = 3$),

sparse spikes begin to appear in the positive half of the LFS driving period, and maintain a certain synchronization with the frequency of the LFS. At this time, the neuron has a strong ability to encode information. As shown in Fig. 2(c), with the further increase of the amplitude of HFS (for $B = 5$), the spikes become denser and the LFS component disappears. This implies the degradation of information encoding, and only appropriate HFS amplitudes can drive neurons for optimal information processing.

To compare globally the different effects of EF and the frequency of HFS on VR, contour plots of neuronal responses Q *versus* HFS amplitude B and frequency ratio N_1 are shown in Fig. 3. Comparing Fig. 3(a) with Fig. 3(b), it can be seen that multiple resonance peaks can be observed when the frequency ratio N_1 is relatively small, especially without EF. As N_1 is increased, HR neuron not exposed to EF changed from multiple resonances to double resonances, and to single vibration resonances at a higher frequency ratio N_1. In contrast, the model of HR neuron exposed to EF switched from multi-resonance to single-resonance earlier. As a result of the participation of the EF, the number of formants can be affected and the effect of the amplitude B and frequency $N_1\omega$ of the HFS is reduced.

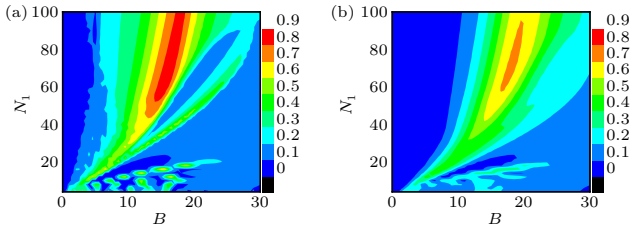


Fig. 3. Contour plot of the response magnitude Q in the parameter space (B, N_1) for the single HR neuron model at $A = 0.3$, $\omega = 0.0314$, $R = 0.00001$, $m = 0.1$; (a) without EF, (b) with EF.

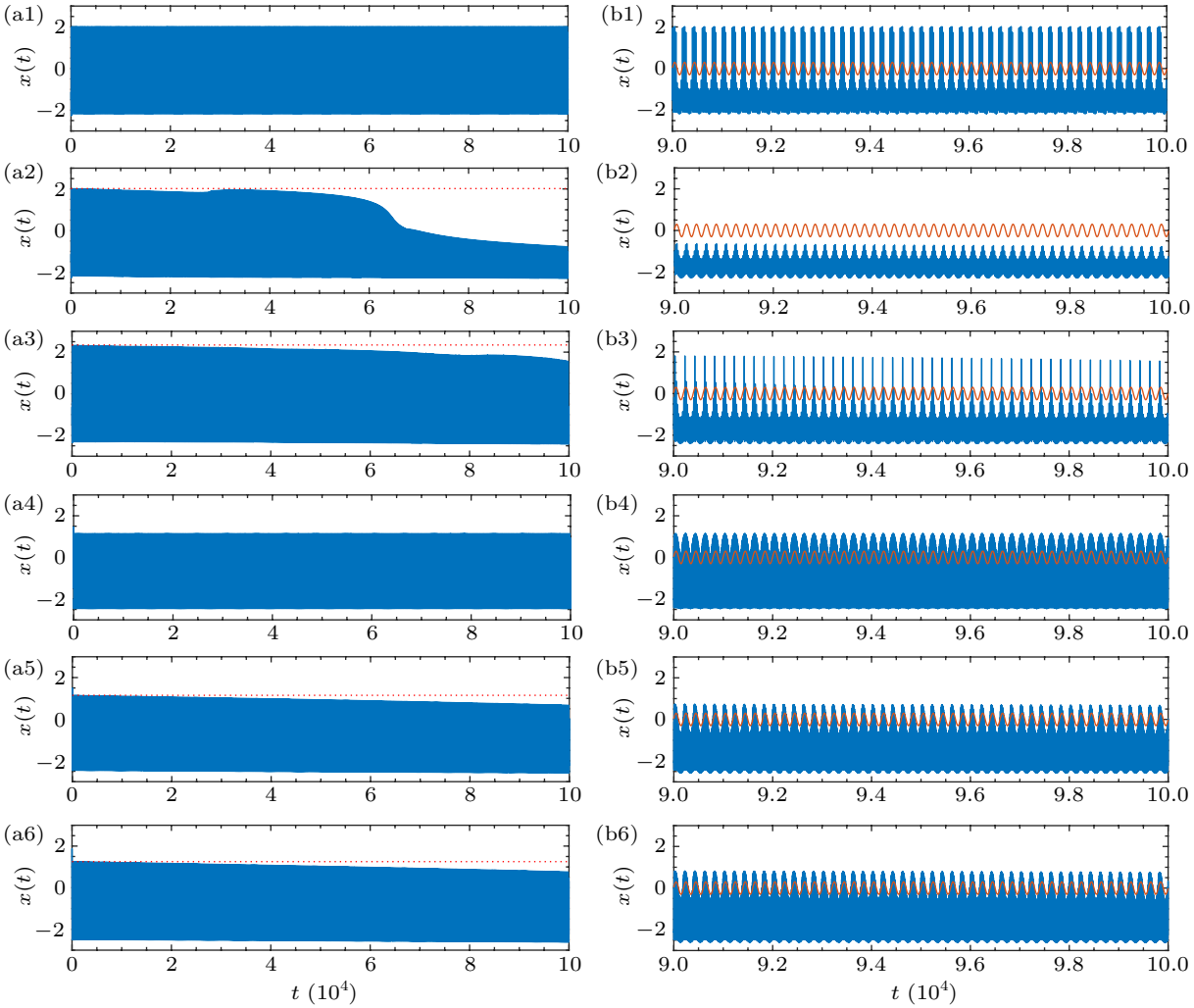


Fig. 4. Time series of the membrane potential and the LFS for different frequency ratios N_1 at $A = 0.3$, $\omega = 0.0314$, $R = 0.00001$, $m = 0.1$; [(a1) and (b1)] $N_1 = 9$, $B = 3$, without EF; [(a2) and (b2)] $N_1 = 9$, $B = 3$, with EF; [(a3) and (b3)] $N_1 = 9$, $B = 4$, with EF; [(a4) and (b4)] $N_1 = 80$, $B = 17.5$, without EF; [(a5) and (b5)] $N_1 = 80$, $B = 17.5$, with EF; [(a6) and (b6)] $N_1 = 80$, $B = 18.5$, with EF.

To further explore the effect of EF on neuronal VR, the evolution of LFS and membrane potential with time over $n = 500$ signal cycles at different frequency ratios N_1 are shown in Fig. 4. As can be seen from the membrane potential sequences, for neuron not exposed to EF (Figs. 4(a1) and 4(a4)), the peak of membrane potential remained unchanged, while the membrane potential spikes of the neuron under the influence of EF decreased significantly with time (Figs. 4(a2) and

4(a5)). Further increasing the amplitude of the high-frequency signal to the maximum resonance response Q, the downward trend of membrane potential is alleviated at this time, and this phenomenon is more obvious when the frequency ratio N_1 is small.

In addition, as can be seen from the more detailed local magnification, for HR neurons not exposed to EF (Figs. 4(b1) and 4(b4)), the burst firing of the neuron is synchronized with the LFS during the positive half-cycle of each LFS. Comparing the six subgraphs, it can be seen that the larger N_1 is, the more spikes are contained in each burst firing of the HR neuron, and the stronger the synchronization with LFS is. However, influenced by EF (Figs. 4(b2), 4(b3), 4(b5), and 4(b6)), the amplitude of the spikes in each burst firing of the neuron decreased with time and the number of spikes contained in the positive half of each LFS drive cycle decreased, which indicates a decreased ability of neuron to encode information. As can be seen from these figures, the inhibitory effect of EF on VR is significant.

To further investigate the effect of EF on neuronal firing frequency, we investigated the spiking pattern of membrane potential upon LFS stimulation. According to the frequency relationship between the frequency of the LFS and the neuronal response, the spiking pattern is divided into p:q mode-locking and chaotic. p:q mode-locking is defined as p action potentials generated by q cycles of stimulation. Pattern 1:1 represents the synchronous response of membrane potentials to low-frequency stimulation signals, and pattern p:1 ($p \geq 2$) represents p-cycle burst synchronization. Chaotic oscillations are aperiodic or irregular responses of membrane potential to input stimuli.

Figure 5 shows the time evolution of neuronal spiking patterns under different HFS. To exclude the influence of parameter B, the time evolution of the spiking pattern when only affected by the electric field is plotted (blue dots in the figure). The red dots show the time evolution of the spiking pattern corresponding to the maximum resonance of the system under the influence of the electric field. It can be seen that the spiking patterns (black dots) of neuron not exposed to EF appear as a fixed mode-locked state over $n = 500$ signal cycles. While affected by EF, the number of spikes in each burst of neurons gradually decreased with time (red dots). Furthermore, comparing the four plots, it can be seen that the initial position of the spike mode increases with increasing frequency ratio N_1, regardless of exposure to EF.

Figure 6 shows the phase diagram and Lyapunov exponent of a neuron driven by dual-frequency periodic signal. Studying the Lyapunov exponent of the system can intuitively analyze the characteristics of chaotic motion. When the neuron was exposed to EF, the orbitals became dense. As shown in Fig. 6(a2), LE_1 is positive, LE_3 is negative, and LE_2 is close to zero, indicating that the three-dimensional system exhibits the characteristics of chaotic motion at this time. In Fig. 6(b2), affected by the electric field, LE_1 and LE_3 are positive, LE_4 is negative, and LE_2 is close to zero, indicating that the four-dimensional system exhibits the characteristics of hyperchaotic motion at this time. However, the maximum Lyapunov exponent of the system did not increase. The possible reason is that due to the polarization effect of the electric field, the membrane potential of neurons prematurely transitioned

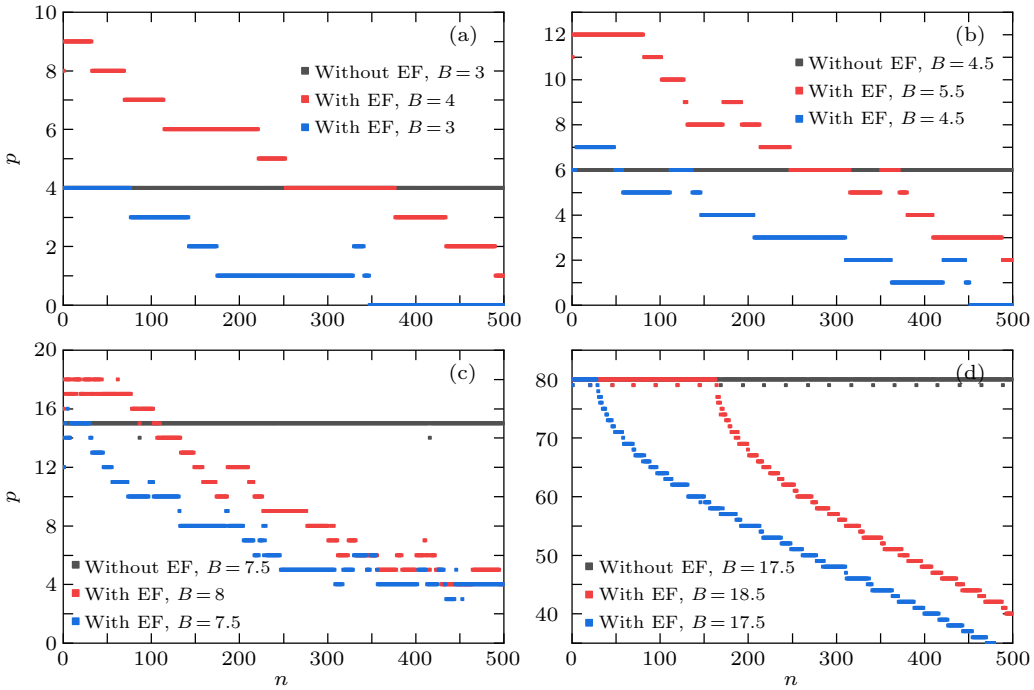


Fig. 5. Spike patterns of single HR neuron over time at $A = 0.3$, $\omega = 0.0314$, $R = 0.00001$, $m = 0.1$; (a) $N_1 = 9$, (b) $N_1 = 12$, (c) $N_1 = 18$, (d) $N_1 = 80$.

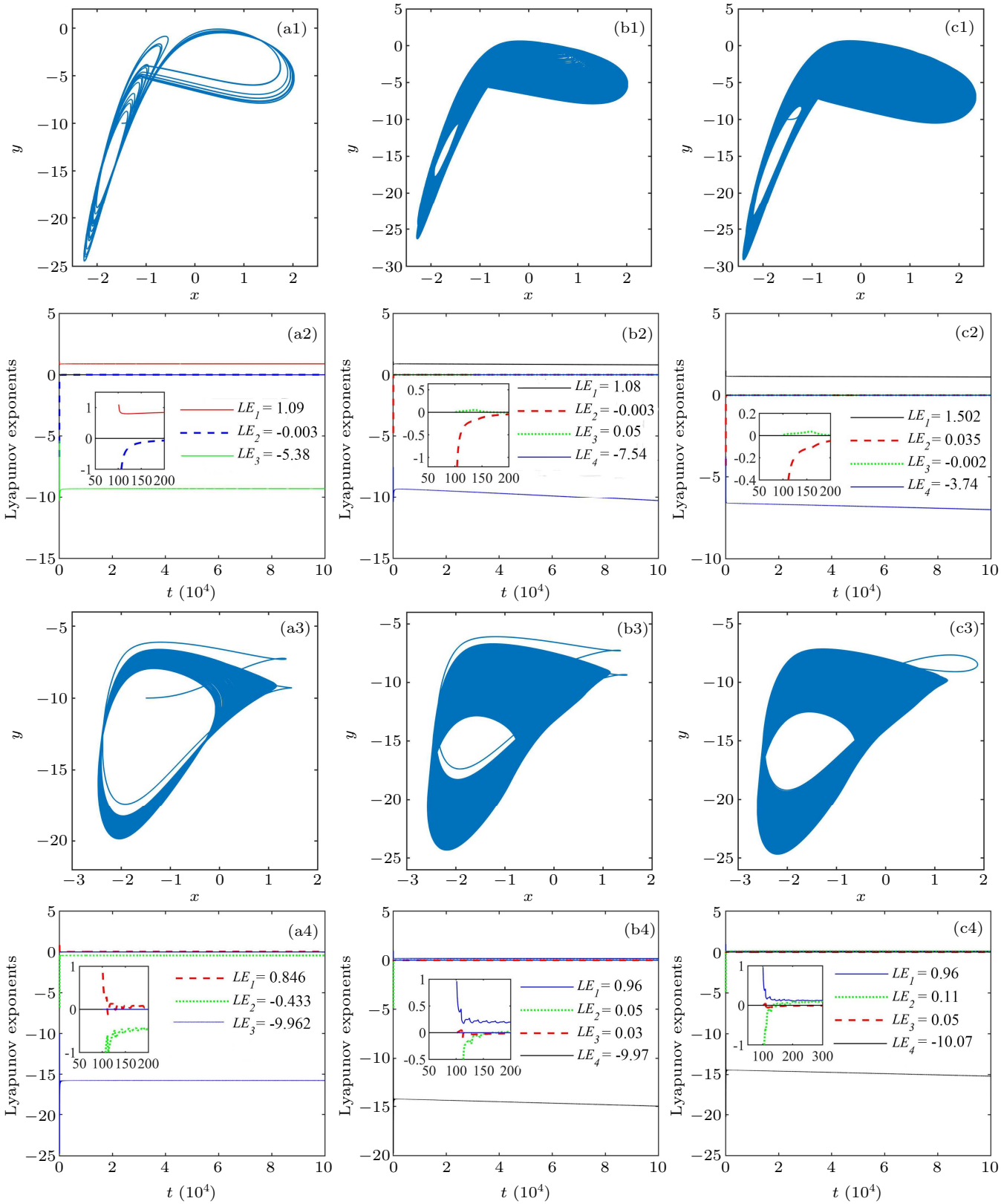


Fig. 6. Attractor profiles drawn and Lyapunov exponent of a single HR neuron at $A = 0.3$, $\omega = 0.0314$, $R = 0.00001$, $m = 0.1$; [(a1) and (a2)] $N_1 = 9$, $B = 3$, without EF; [(b1) and (b2)] $N_1 = 9$, $B = 3$, with EF; [(c1) and (c2)] $N_1 = 9$, $B = 4$, with EF; [(a3) and (a4)] $N_1 = 80$, $B = 17.5$, without EF; [(b3) and (b4)] $N_1 = 80$, $B = 17.5$, with EF; [(c3) and (c4)] $N_1 = 80$, $B = 18.5$, with EF.

to a subthreshold oscillatory state (Fig. 5(a)), which weakened the chaotic discharge of the system. As shown in Fig. 6(c2), the maximum resonance response is achieved by increasing the amplitude of the high-frequency signal. At this time, the maximum lyapunov exponent of the system increases significantly, and the degree of chaos further increases. When $N_1 = 80$, under the influence of the electric field, the maximum Lyapunov exponent increases and the degree of chaos

increases. That is, the modulation of electrical activity patterns by EF is significant.

This phenomenon suggests that the inhibitory effect of EF on VR is caused by two factors, reducing the membrane potential and disrupting the regular spiking pattern of HR neuron. EF attenuated the VR of neuron, reduced the ability of neuron to encode and detect weak signals, and the effect of attenuating multiple vibrational resonances was more pronounced when the ratio of frequencies N_1 was small. The possible reason is that the time-varying electric field generated by the polarization of the medium affects the transmembrane movement of charged ions, so that the firing of neurons becomes disordered, and the accumulation of the electric field causes the membrane potential to decrease with time. In fact, maintaining charge balance during deep brain stimulation therapy is an important factor in ensuring safe stimulation with functional electrical stimulators. Over time, excessive charge accumulation can lead to nerve tissue destruction and electrode dissolution.[53]

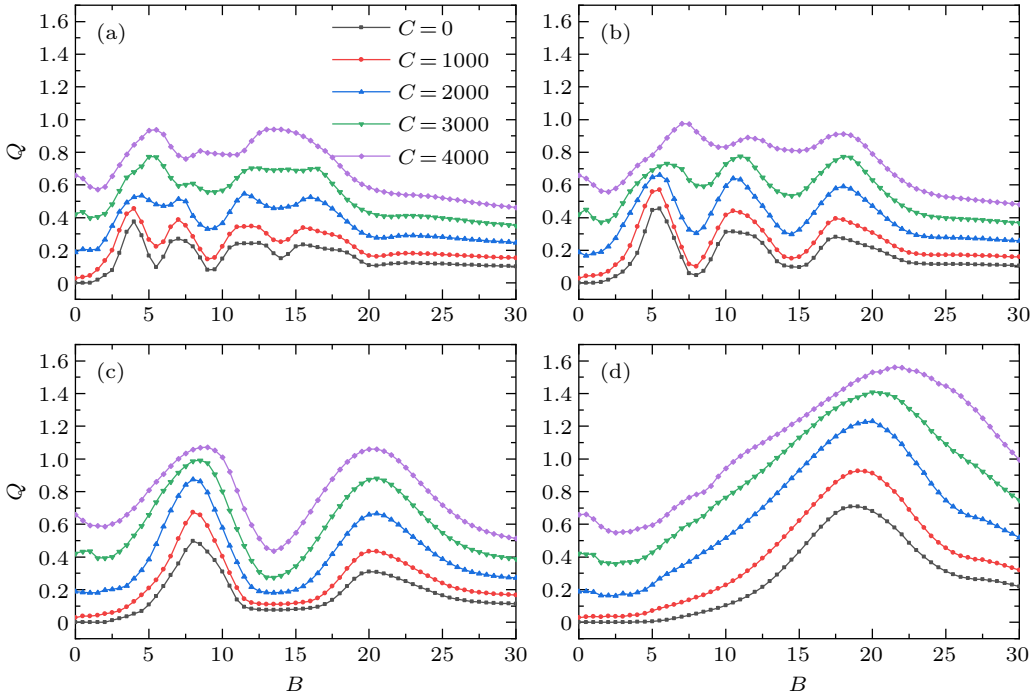


Fig. 7. Dependence of response amplitude Q on HFS amplitude B under different EF strengths C and frequency ratios N_1 at $A=0.3$, $\omega=0.0314$; (a) $N_1=9$, (b) $N_1=12$, (c) $N_1=18$, (d) $N_1=80$.

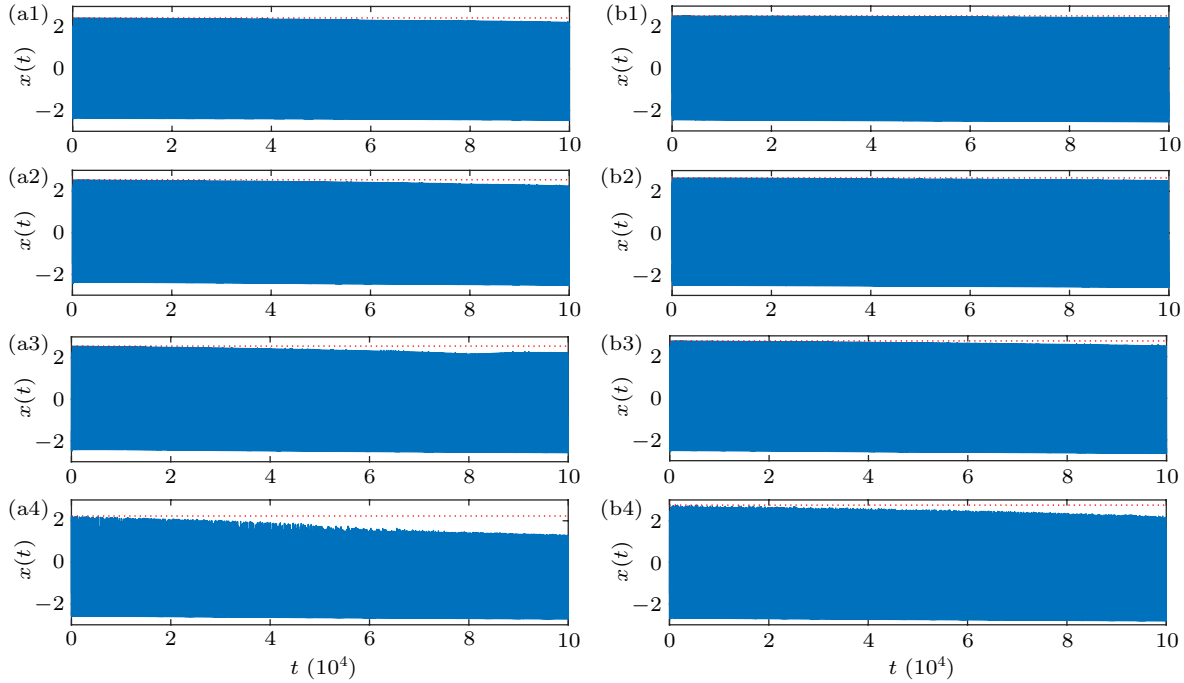


Fig. 8. Membrane potential of HR neuron and LFS evolution over time with $A=0.3$, $\omega=0.0314$; (a1) $C=2000$; (b1) $C=4000$, $N_1=9$, $B=4$; (a2) $C=2000$; (b2) $C=4000$, $N_1=12$, $B=5.5$; (a3) $C=2000$; (b3) $C=4000$, $N_1=18$, $B=8$; (a4) $C=2000$; (b4) $C=4000$, $N_1=80$, $B=18.5$.

Next, we study the dynamic response of neurons when a periodic external EF $E_{\rm ext} = C\cos(N_2\omega t)$ is applied. Again, we choose appropriate frequency ratios N_1 to ensure comparisons are made at different numbers of formants. Figure 7 shows the relationship between the response amplitude Q of neuron and the amplitude B of HFS under different electric field strengths C. It can be observed that regardless of the magnitude of the frequency ratio N_1, the increase of the electric field strength C on the response amplitude Q of the neuron is obvious. Interestingly, the response magnitude Q curves gradually flatten with increasing C. For lower frequency ratios N_1, the number of formants also decreases with increasing C.

To further explore the effect of external EF on neuron VR, the time evolution of membrane potential and LFS over $n = 500$ signal cycles under different EF strengths is plotted in Fig. 8. On the time scale of $n = 500$ cycles, the downward trend of the membrane potential peak was slowed by the external EF.

Discussing further, we plot the peak distribution of membrane potential (MPD) of neurons over $n = 500$ signal cycles under an external periodic EF in Fig. 9. Since information transmission and encoding in neurons is achieved by positive spiking potentials, neuronal oscillations below the threshold cannot be used to transmit any information, so we mainly focus on the positive half of neuronal spiking signals. It can be observed that the external EF makes the peak of the membrane potential more concentrated near the higher potential, and the higher the strength of the external EF, the more obvious this concentration. This corresponds to the larger membrane potential peak in Fig. 8.

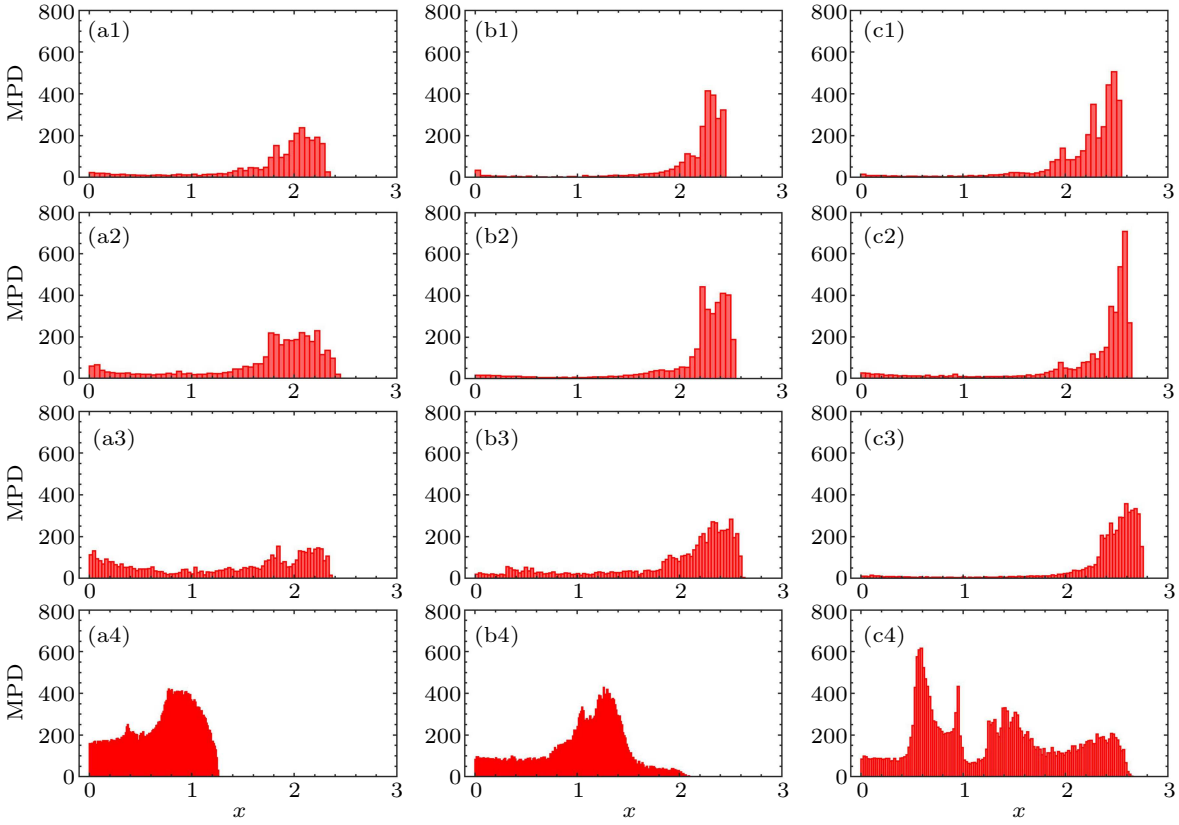


Fig. 9. HR neuron membrane potential peak distribution with $A = 0.3$, $\omega = 0.0314$; (a1) $C = 0$; (b1) $C = 2000$; (c1) $C = 4000$, $N_1 = 9$, $B = 4$; (a2) $C = 0$; (b2) $C = 2000$; (c2) $C = 4000$, $N_1 = 12$, $B = 5.5$; (a3) $C = 0$; (b3) $C = 2000$; (c3) $C = 4000$, $N_1 = 18$, $B = 8$; (a4) $C = 0$; (b4) $C = 2000$; (c4) $C = 4000$, $N_1 = 80$, $B = 18.5$.

Considering the effects of internal and external EF on neuronal firing activity, it can be seen that the internal EF reduces the number of spiking contained in each LFS driving cycle, and the internal EF gradually decreases the peak value of membrane potential due to the effect of charge accumulation. The external EF weakened this downward trend to a certain extent, and increased the membrane potential of neurons, so that neurons transmit more information energy in the same time range, which enhanced VR.

After studying the effect of the external EF strength C on the output response, we are also interested in the effect of the frequency $N_2\omega$ of the external EF on the output response. Therefore, in a single HR neuron model, the response amplitudes Q as a function of frequency ratio N_2 are shown in Fig. 10. Interestingly, for different frequency ratios N_1 and EF strengths C, we found that the response amplitude Q of neurons has a clear screening effect on the frequency $N_2 = 1$, and the higher the strength C of the external EF, the more obvious the screening effect. This indicates a strong frequency dependence between the external EF and LFS.

In the presence of subthreshold electrical stimulation and the periodic external electric field ($C = 4000$), the angular frequency of the periodic electric field was varied to detect electrical activity, and the results are shown in Fig. 11. For the smaller frequency ratio ($N_2 = 0.5$) in Fig. 11(a), the corresponding period of neuronal electrical activity is not synchronized with the period of LFS. When the frequency of the EF is increased ($N_2 = 1$), as shown in Fig. 11(b), the burst firing of neurons maintains a high synchronization with the LFS. Continue to increase the electric field frequency, as shown in Fig. 11(c), $N_2 = 2$; Fig. 11(d), $N_2 = 3$, at this time, the correlation between the electrical activity of neurons and LFS is weakened. The results show that tuning the frequency of the periodic external EF can trigger multiple electrical activity patterns, and the electrical activity of HR neurons has a strong dependence on the electric field frequency of $N_2 = 1$.

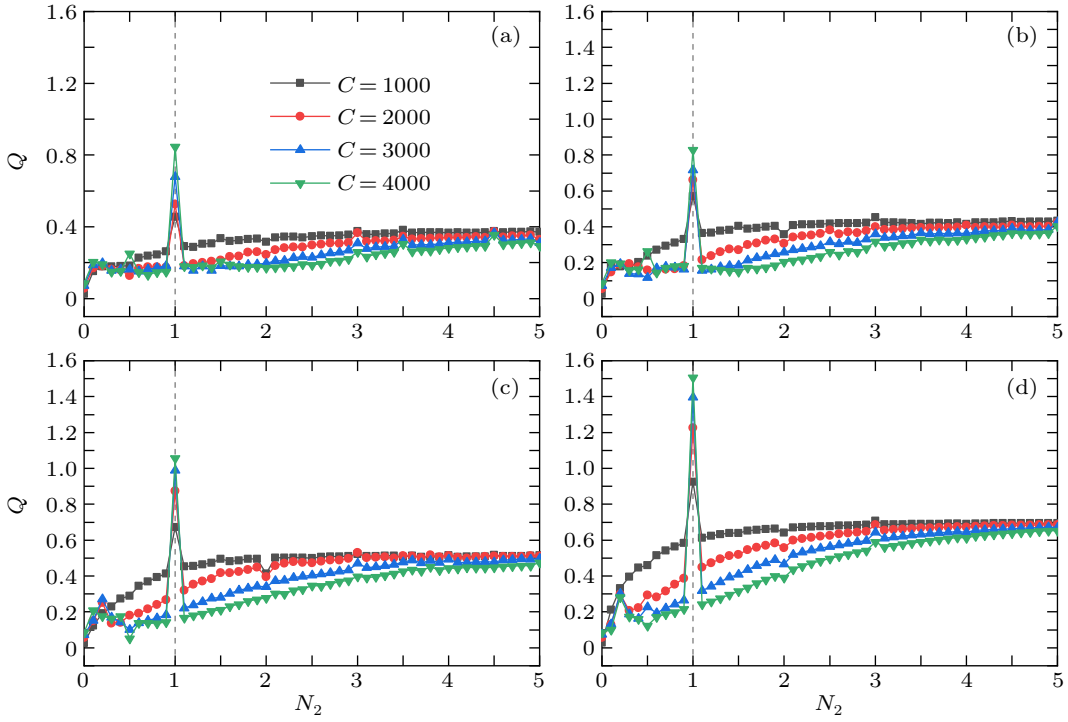


Fig. 10. Response amplitudes Q as a function of frequency ratio N_2 at $A = 0.3$, $\omega = 0.0314$; (a) $N_1 = 9$, $B = 4$; (b) $N_1 = 12$, $B = 5.5$; (c) $N_1 = 18$, $B = 8$; (d) $N_1 = 80$, $B = 18.5$.

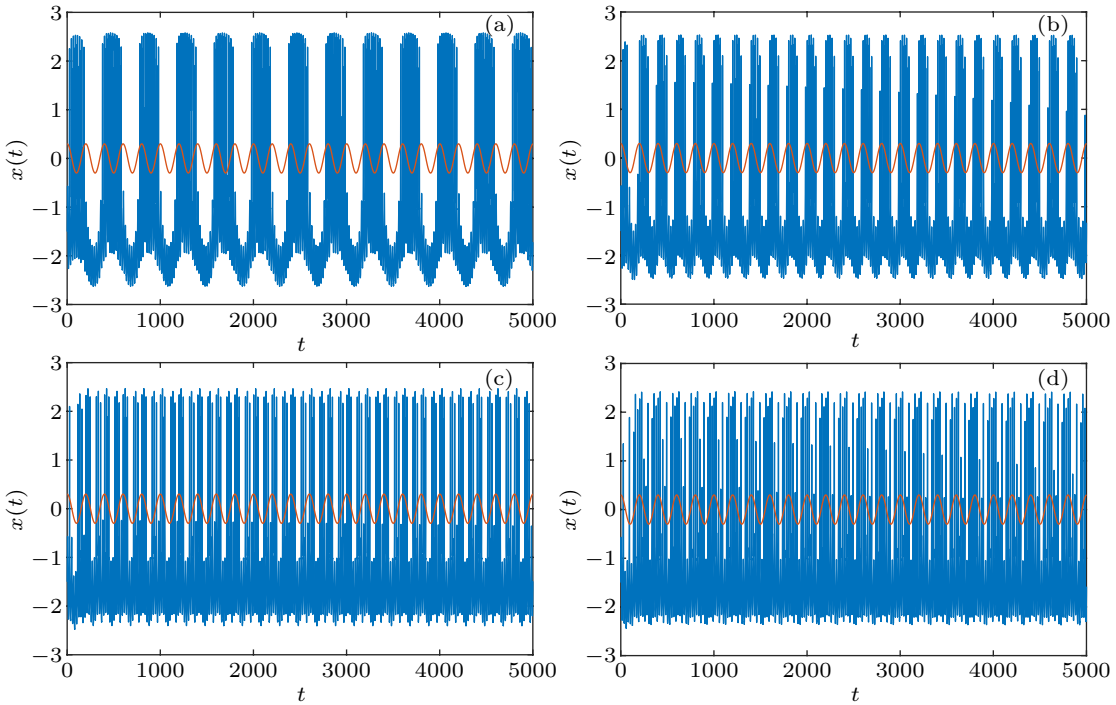


Fig. 11. Time-dependent changes in membrane potential and LFS of single HR neurons with different frequency ratios N_2 at $A = 0.3$, $\omega = 0.0314$, $N_1 = 9$, $B = 4$, $C = 4000$; (a) $N_2 = 0.5$, (b) $N_2 = 1$, (c) $N_2 = 2$, (d) $N_2 = 3$.

3.2. VR in coupled Hindmarsh–Rose neurons model

It is well known that synaptic connections play an important role in energy exchange and signal propagation between neurons, and electrical synapses through gap junctions can ensure fast responses between neurons. Figure 12 shows contour plots of response amplitude Q *versus* HFS amplitude B and frequency ratio N_1 for an HR neuron model of electrical synapse coupling. In this paper, $g_2 = 0$ indicates no electric field coupling. The response magnitudes Q of the coupled neuron model exhibit similar characteristics to those of the single neuron. Coupled neurons that were not exposed to EF exhibited a pronounced MVR at lower frequency ratios N_1, becoming a double-peak resonance with increasing N_1 and a single resonance with larger N_1. Affected by EF, the MVR of coupled neurons weakened, and the response amplitude changed from multiple resonances to single resonances earlier with the increase of N_1. Furthermore, unlike the response of individual HR neuron to LFS, coupled neurons completed signal detection within a narrow range of HFS amplitudes B.

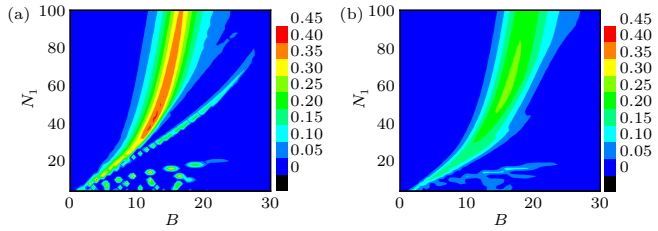


Fig. 12. Contour plot of the response amplitude Q of the coupled HR neuron model in the parameter space (B, N_1) of $g_1 = 1$, $g_2 = 0$, $A = 0.3$, $\omega = 0.0314$; (a) without EF, (b) with EF.

Next, contour plots of response amplitude Q *versus* coupling strength g_1 and HFS amplitude B in the bidirectionally coupled HR neuron model are plotted in Fig. 13. It can be seen that, with or without EF, the magnitude Q of the response and the coupling strength g_1 show an obvious proportional relationship. When it is smaller, the resonance effect is weak, and the increase of g_1 increases the response amplitude Q, and has no effect on the number of formants.

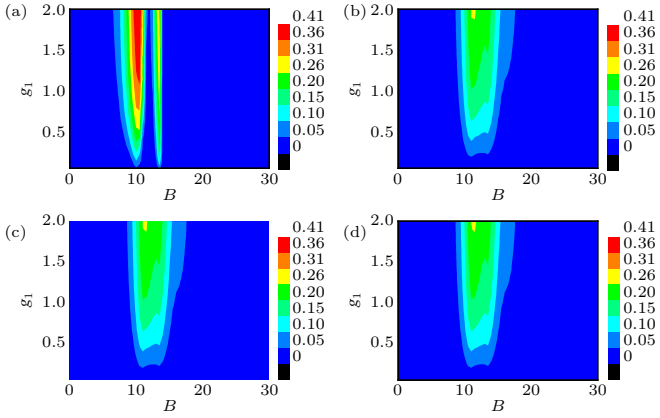


Fig. 13. Contour plots of the response magnitude Q for the coupled HR neuron model in the parameter space (B, g_1) of $N_1 = 30$, $A = 0.3$, $\omega = 0.0314$; (a) without EF; (b) with EF, $g_2 = 0$; (c) with EF, $g_2 = 2$; (d) with EF, $g_2 = 4$.

Existing studies have shown that electromagnetic coupling can affect the electrical synaptic coupling between neurons.[55,56] Therefore, studying the effect of electric field coupling on VR is important for understanding neural electrical activity. Figure 14 shows a contour plot of response amplitude *versus* coupling strength g_2 and HFS amplitude B for HR neurons coupled by symmetric activation electric fields. It can be seen from Figs. 13(b)–13(d) and 14 that the EF coupling has little effect on VR. From a deeper perspective, whether EF coupling can affect the electrical activity of neurons deserves further investigation.

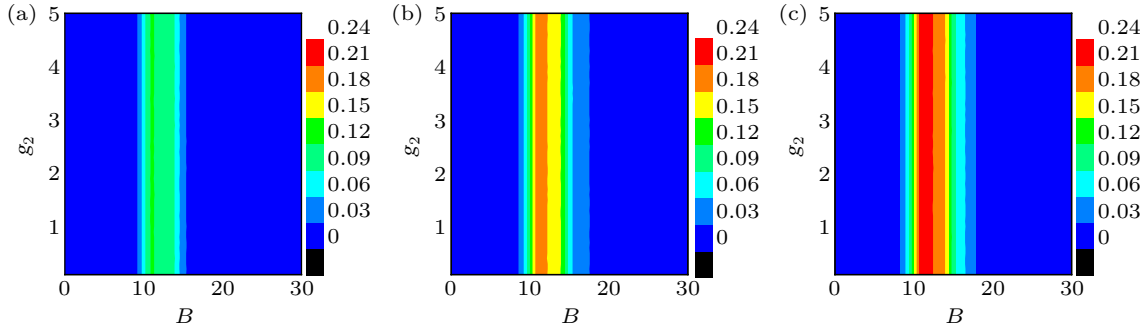


Fig. 14. Contour plots of response magnitude Q in the parameter space (B, g_2) of $N_1 = 30$, $A = 0.3$, $\omega = 0.0314$ for an EF-coupled HR neuron; (a) $g_1 = 0.5$, (b) $g_1 = 1$, (c) $g_1 = 1.5$.

4. Conclusion

The effect of the electric field on the vibrational resonance of a single Hindmarsh–Rose neuron model and two bidirectionally coupled Hindmarsh–Rose neuron models was investigated. For the single Hindmarsh–Rose neuron model, the internal electric field reduces membrane potential and impairs fixed phase-locked patterns. Thus, the internal electric field suppresses the vibrational resonance, indicating impaired detection of low-frequency signals by neurons. The periodic external electric field significantly increased the membrane potential of neuronal and enhanced the vibrational resonance. Interestingly, we found that a distinct phase-locking mode only appeared when the frequency of the external electric field was the same as that of the low-frequency signal.

The effects of the electric field on the coupled Hindmarsh–Rose neuron model have similarities to that of a single neuron. Furthermore, we can enhance the vibrational resonance by increasing the electrical synaptic coupling strength regardless of the presence of an electric field, while the electric field coupling has no appreciable effect on the vibrational resonance of the system.

The clinical application of deep brain stimulation (DBS) is one of the important advances in neuroscience, however, the further application of this technology still needs to solve some problems.[57] The specific working mechanism of DBS is still under debate, and current studies suggest that the stimulatory effect of DBS occurs at the ionic and cellular levels.[58,59] At the ionic level, electrical stimulation redistributes charged particles inside and outside the cell membrane and generates polarized electric fields that further influence action potentials.[60] Electric fields are ubiquitous in our surrounding environment. Studying the transmission of electric field-induced action potentials helps to understand the mechanism of action of electrical stimulation. Although the effect of electric field on neuronal vibration resonance is obtained based on numerical simulation in this paper, it is hoped that this study can enrich neuroscience research, especially to establish a certain theoretical basis for deep brain stimulation and vibration resonance.

Acknowledgments

Project supported by the National Natural Science Foundation of China (Grant Nos. 51737003 and 51977060) and the Natural Science Foundation of Hebei Province, China (Grant No. E2011202051).

References

[1] Benzi R, Sutera A and Vulpiani A 1981 *Physica A* **14** 453
[2] Benzi R, Parisi G, Sutera A and Vulpiani A 1982 *Tellus* **34** 10
[3] Benzi R 2010 *Nonlinear Process Geophys* **17** 431
[4] Mikhaylov A N, Guseinov D V, Belov A I, *et al.* 2021 *Chaos, Solitons and Fractals* **144** 110723
[5] Bai C, Du L and Mei D 2009 *Cent. Eur. J. Phys.* **7** 601
[6] Wang C J 2004 *Phys. Scr.* **80** 065004
[7] Han Q, Yang T and Zeng C, Wang H, Liu Z, Fu Y, Zhang C and Tian D 2014 *Physica A* **408** 96
[8] Zhang R F, Cheng Q H and Xu D H 2015 *Acta Phys. Sin* **64** 024211 (in Chinese)
[9] Chizhevsky V N and Giacomelli G 2006 *Phys. Rev. E* **73** 022103
[10] Hänggi P 2002 *Chempluschem* **3** 285
[11] Landa P S and McClintock P V E 2000 *J. Phys. A: Math. Theor.* **33** L433
[12] Zaikin A A, López L, Baltanás J P, Kurths J and Sanjuán M A F 2002 *Phys. Rev. E* **66** 011106
[13] Chizhevsky V N, Smeu E and Giacomelli G 2003 *Phys. Rev. Lett.* **91** 220602
[14] Ghosh S and Ray D S 2013 *Phys. Rev. E* **88** 042904
[15] Carroll T L and Pecora L M 1993 *Phys. Rev. Lett.* **70** 576
[16] Nobukawa S and Shibata N 2019 *Sci. Rep.* **9** 4990
[17] Baysal V, Saraç Z and Yilmaz E 2019 *Nonlinear Dyn.* **97** 1275
[18] Yao Y, Ma J, Gui R and Cheng G 2021 *Chaos* **31** 023103
[19] González-Miranda J M 2007 *Int. J. Bifur. Chaos* **17** 3071
[20] Hodgkin A L and Huxley A F 1952 *J. Physiol.* **117** 500
[21] Noble D 1960 *Nature* **188** 495
[22] Chua L, Sbitnev V and Kim H 2012 *Int. J. Bifur. Chaos* **22** 1230011
[23] Hu X and Liu C 2019 *Nonlinear Dyn.* **97** 1721
[24] FitzHugh R 1969 *Bioeng* **1** 85
[25] Morris C and Lecar H 1981 *Biophys. J.* **35** 193
[26] Hindmarsh J L and Rose R M 1982 *Nature* **296** 162
[27] Prescott S A, Ratté S, De Koninck Y and Sejnowski T J 2006 *J. Neurosci.* **26** 9084
[28] Wiesenfeld K and Jaramillo F 1998 *Chaos* **8** 539
[29] Shepherd G M 2004 *OUP*
[30] Song X, Wang H and Chen Y 2018 *Nonlinear Dyn.* **94** 141
[31] Han C, Qin Y and Qin Q 2019 *Physica A* **523** 204
[32] Li H, Sun X and Xiao J 2018 *Chaos* **28** 043113
[33] Douglass J K, Wilkens L, Pantazelou E and Moss F 1993 *Nature* **365** 337
[34] Lv M, Wang C, Ren G, Ma J and Song X 2016 *Nonlinear Dyn.* **85** 1479
[35] Bhargavan M 2008 *Health. Phys.* **95** 612
[36] Shneider M N and Pekker M 2013 *J. Appl. Phys.* **114** 104701
[37] Oberschleissheim 2020 *Health. Phys.* **118** 483
[38] Capelli E, Torrisi F, Venturini L, Granato M, Fassina L, Lupo G F D and Ricevuti G 2017 *J. Healthc. Eng.* **2017** 2530270
[39] Ahmad R H M A, Fakhoury M and Lawand N 2020 *Curr. Alzheimer. Res.* **17** 1001
[40] Fisher R, Salanova V, Witt T, *et al.* 2010 *Epilepsia* **51** 899
[41] Muñana K R 2013 *Top. Companion. Anim. M* **28** 67
[42] Yao Y, Su C and Xiong J 2019 *Physica A* **531** 121734
[43] Ge M, Lu L, Xu Y, Mamatimin R, Pei Q and Jia Y 2020 *Chaos, Solitons and Fractals* **133** 109645
[44] Baysal V and Yilmaz E 2020 *Physica A* **537** 122733
[45] Ma J, Zhang G, Hayat T and Ren G 2019 *Nonlinear Dyn* **95** 1585
[46] Hou Z, Ma J, Zhan X, Yang L and Jia Y 2021 *Chaos, Solitons and Fractals* **142** 110522
[47] Rubin J E and Terman D 2004 *J. Comput. Neurosci.* **16** 211
[48] Sanders T H 2017 *Front. Integr. Neurosci.* **11** 24
[49] Stefani A, Trendafilov V, Liguori C, Fedele E and Galatib S 2017 *Prog. Neurobiol.* **151** 157
[50] Wouapi K, Fotsin B H, Louodop F P, Feudjio K F, Njitacke Z T and Hermann Djeudjo T 2020 *Cogn. Neurodyn.* **14** 375
[51] Deng B, Wang J and Wei X 2009 *Chaos* **19** 013117
[52] Wu X X, Yao C and Shuai J 2015 *Sci. Rep.* **5** 1
[53] Merrill D R, Bikson M and Jefferys J G R 2005 *J. Neurosci. Methods* **141** 171
[54] Lv M, Ma J, Yao Y G and Alzahrani F 2019 *Sci China Technol. Sci.* **62** 448
[55] Xu Y, Jia Y, Ma J, Hayat T and Alsaedi A 2018 *Sci. Rep.* **8** 1
[56] Ma J, Wu F, Alsaedi A and Tang J 2018 *Nonlinear Dyn.* **93** 2057
[57] Lozano A M, Lipsman N, Bergman H, Brown P, Chabardes S, Chang J W, Matthews K, McIntyre C C, Schlaepfer T E, Schulder M, Temel Y, Volkmann J and Krauss J K 2019 *Nat. Rev. Neurol.* **15** 148
[58] Lozano A M and Lipsman N 2013 *Neuron* **77** 406
[59] Ashkan K, Rogers P, Bergman H and Ughratdar I 2017 *Nat. Rev. Neurol.* **13** 548
[60] Groome J R 2014 *Voltage Gated Sodium Channels* pp. 7–31